New Solar Physics with Solar-B Mission
ASP Conference Series, Vol. 369, 2007
K. Shibata, S. Nagata, and T. Sakurai

Investigation of Reconnection in the Solar Corona by Numerical Simulation based on Solar-B Observations

Jörg Büchner

Max-Planck-Institut für Sonnensystemforschung, 37191 Katlenburg-Lindau, Germany

Abstract. Solar-B observations are going to provide rich information which will enable a better understanding of magnetic reconnection in the solar atmosphere. So far different models exist of reconnection in three dimensions with different consequences for flare and CME triggering as well as for solar particle acceleration. Most of these models are qualitative, cartoon-like, i.e. they can neither be verified nor can they be falsified quantitatively by observations. Numerical simulation approaches are necessary to describe the nonlinear, nonlocal and ranging over extremely different scales physical processes, which are not directly observable. We discuss key aspects which have to be taken into account in order to develop appropriate forward simulation models which are able to specify the nature of solar reconnection by a direct comparison with Solar-B observations. As a starting point we discuss how to use the vector magnetic field information provided by SOT as an initial condition for the simulations. We further consider the use of the time series of SOT vector magnetic field observations to derive appropriate boundary conditions simulation models able to describe the energy input into the chromosphere and corona. Further, an appropriate coupled plasma – neutral gas model is suggested, able to describe the consequences of the sub-photospheric energy input for reconnection causing electron acceleration, indirectly observable by XRT, and plasma heating, observable by EIS. Since location, triggering conditions and strength of reconnection depend on microscopic dissipation processes, we shortly review the state that appropriate transport coefficients for solar coronal conditions. Finally, we show by an example that different resistivity models might reveal completely different locations and size of three-dimensional reconnection and the corresponding electric fields in the solar corona, so that they can be verified by solar B-observations.

1. Introduction

The four main objectives of the Solar-B mission are the most striking open questions in solar physics: creation and destruction of the Sun's magnetic field, modulation of the solar luminosity, conversion of solar magnetic energy into UV and X-ray radiation and the causes of solar eruptions, which all address in one or another way magnetic reconnection (Tsuneta, 1996; Shibata, 1998). Indeed, solar magnetic reconnection is not well understood, yet. Open is the reason for its initiation (triggering condition), its location, its structure and dynamics in three dimensions, its role in solar eruptions, i.e. whether it is primary or secondary, how fast it can become and how much energy is converted into particle acceleration, plasma flow energy and heating. The Solar-B mission is well suited to improve our understanding of reconnection in the solar corona. Since existing forward models are not sufficiently quantitative to allow their direct verification

by observations, better models have to be developed for taking out most from Solar-B observations.

The lowest order approximation to model the magnetic fields of the corona is a formal mathematical extrapolation of the photospheric magnetic field (Sakurai, 1989). Such approach assumes that the coronal magnetic field is force-free ($rot\vec{B} = \alpha\vec{j}$) or even current-free (potential field approximation, $rot\vec{B} = 0$). Obviously, this does not allow, in principle, to consider a dissipative physical process like reconnection and to address the open questions its about cause, nature and consequences. The question arises, which more appropriate modelling approach should one take? The global change of magnetic connectivity as well as flares and CME ejections require a large scale treatment, a fluid approach. Also, one wants to understand the physics of the corona in its interaction with the chromosphere and the photosphere. In contrast to the chromosphere the coronal plasma is to a large extent an ideally conducting fluid. A quantitative measure for the plasma idealness versus resistivity is the magnetic Reynolds number $R_m = \mu_0\ L\ v/\eta$. With the vacuum magnetic permeability $\mu_0 = 4\pi\,10^{-7}$ Vs/Am being a constant, the magnetic Reynolds number depends on the characteristic size of the region L, the characteristic plasma velocity v and its electric resistivity η. For a typical flare size $L = 10^7\ m$, a typical flow velocity 1 km/s and a collisional resistivity $\eta_\perp \cong 10^{-4} ln\Lambda\ T_e^{-3/2}\ \Omega m$ (Spitzer, 1956) (where $ln\Lambda$ is the Coulomb-logarithm -usually $20 - 30$- and T_e the electron temperature in eV) for a $T_e = 100$ eV $= 10^6$ K hot coronal plasma, i.e. for $\eta = 10^{-7}\ \Omega$m, the Reynolds number is of the order of 10^{10}! This means that the flare energy release cannot be explained by Spitzer-type collisional resistivity. Magnetic reconnection is able to enhance the release of magnetic and plasma flow energy taken from large regions through a small non-ideal plasma region (Priest & Forbes, 2000). Reconnection is characterized by a change of the magnetic connectivity through such non-ideal plasma region (Axford, 1984). Hence, for reconnection it is sufficient if the magnetic Reynolds number drops just locally to small values of the order of unity to allow the conversion of magnetic field and slow large scale plasma energy to a buildup of electric fields, fast, Alfvénic, plasma flows, heating and particle acceleration to high energies. Reconnection, therefore, needs local dissipation due to small-scale, kinetic processes exceeding the weak Spitzer-type collisional dissipation, to cause large scale restructuring and energy release in the corona.

Since the plasma flow velocity which enters R_m is known from observation there are two ways to reach small local magnetic Reynolds numbers: small non-ideal plasma regions (small L) and a large effective resistivity η_{eff}, exceeding the collisional Spitzer value by orders of magnitude. While in the dense chromospheric plasma the resistivity is large due to additional collisional terms, altogether combined in the so called "Cowling resistivity" (Cowling, 1957), in the corona only collective wave-particle interaction phenomena may enhance the resistivity to sufficiently large values (Priest, 1982), which have to be derived from microscopic theories (see, e.g., Büchner & Elkina, 2006a).

Since, therefore, reconnection is an essentially nonlocal, multi-scale process combining kinetic and fluid scales, numerical simulation is necessary to derive verifiable quantitative consequences of the resistivity models in order to test them on Solar-B data. Yokoyama & Shibata, (1994), for example, considered the consequence of different macroscopic resistivity models of the microphysical

dissipation mechanisms. They fluid-simulated a two-dimensional magnetohydrodynamic (MHD) buoyancy instability applying alternatively either an uniform resistivity $\eta = const. = \eta_o$ or a resistivity, switched on after the relative drift of ions and electrons, i.e. the current carrier velocity u_{ccv}, calculated as current density j, divided by the charge density ρ, i.e. as $u_{ccv} = j/\rho_e$, exceeds a certain threshold u_{crit}. They found that already in two dimensions the reconnection rate is not uniquely determined by the driving process, but that it strongly depends on the resistivity model taken near the (2D) neutral point. For example, in their calculations the reconnection rate increased with an increasing threshold for the switch-on of the resistivity. Another investigation of the influence of macroscopic resistivity models on 2D reconnection was carried out by Roussev et al., (2002). They confirmed that the threshold, at which resistivity switches on, influences the dynamics of reconnection: higher threshold values provide a localized on-off effect of patchy diffusion. They also found that for a given resistivity value the amount of Joule heating is larger for smaller threshold values.

The properties of reconnection geometry in the real three-dimensional solar atmosphere has still to be determined, e.g., whether it contains a magnetic null point or, if not, how finite-B reconnection looks like and where it is located and how it depends on the macroscopic resistivity model (see, e.g., Büchner, 2006). In order to find out by forward modelling, where, when and how reconnection takes place in the solar corona, one should start with the fact that the energy dissipated by reconnection in the solar atmosphere originates from the interior of the Sun. Hence, it has to be transported through the photosphere, the natural boundary for coronal simulation models. SOT onboard Solar-B provides the full vector magnetic field information for the photosphere, with a diffraction limited resolution of 0.25" (or 175 km on the Sun), a sensitivity of 1-5 G for the longitudinal and of 30-50 G for the transverse magnetic field component. It allows to follow the dynamical evolution of the magnetic field, of the photospheric currents and plasma motion with a time resolution of 5 minutes. The detectable change of the magnetic energy of an active regions will be about 10^{30} erg. SOT observations provide an invaluable input information for the forward modelling of coronal heating processes, the triggering of solar eruptions and the particle acceleration to high energies. For the latter, as for reconnection the microscopic buildup and balancing of electric fields has to be taken into account. Reconnection leads to particle acceleration, indirectly observable by XRT. A combination of the microphysics of electric field generation with the macrophysics of plasma flows is also necessary to model solar reconnection and to derive the energy conversion into heat, causing EUV radiation observable by EIS. Hence, multi-scale coupling models have to be developed in which the small scale dissipation processes are coupled to the macroscopic, large scale plasma flows in a consistent way. First of all, however, one should start with an equilibrium based on the observed photospheric magnetic field. In section 2. we discuss the construction of initial equilibria consistent with SOT observations. Further one has to impose appropriate boundary conditions consistent with the photospheric plasma motion. In section 3. we first review existing methods for deriving the photospheric plasma motion from magnetic field observations and then discuss how to implement appropriate boundary condition for the simulation. In section 4. we provide a set of fluid equations describing a plasma-neutral gas model of chromosphere and corona. The dissipation arises at microscopic scales and has

to be treated kinetically. In section 5. we consider the most appropriate macroscopic resistivity models based on latest kinetic simulation results necessary to correctly treat the microphysics of collisionless coronal plasmas. In section 6. we give an example of combining the microscopic and macroscopic aspects of coronal reconnection in a forward model of the location and shape of the reconnection region in dependence on different resistivity models. We demonstrate the crucial role which the resistivity model plays in 3D reconnection for locating reconnection. Finally, in section 7. we draw conclusions about the next steps to be gone in developing forward models in order to utilize best all the brilliant opportunities, Solar-B will provide.

2. Initial Conditions

Since in the corona $\beta = 8\pi n k_B T/B^2 \ll 1$, i.e. since the kinetic pressure is much smaller than the magnetic pressure, the initial magnetic field configuration can be obtained independent on the plasma distribution. The most reliable information for constructing an initial magnetic field close to reality is the observed photospheric magnetic field. Assuming force-free conditions one can solve the resulting elliptic partial differential equation for the magnetic field or its potentials by combining the photospheric field information with appropriate boundary conditions. One can start, e.g. with the most accurately determined line-of-sight component of the photospheric magnetic field, at least, if no information about the photospheric currents (i.e. no vector magnetic field information) is available. In such current-free, potential approach one finds a lowest energy state of the coronal magnetic field, neglecting force-free parallel currents and, of course, the cross-field current sheets recently detected (Solanki et al., 2003).

Other than, e.g., the Seehafer, (1978) solution for a force-free field the compatibility with magnetohydrodynamic (MHD) boundary conditions requires a well defined local symmetry of the boundary conditions for the magnetic field, in particular, the symmetry conditions for the magnetic field and for the current density have to be the same. We currently derived a way how this can be done in a compatible with MHD boundary conditions (Büchner et al., 2004a, 2005; Otto et al., 2006). There we derived an extrapolation scheme, compatible with the requirements of MHD. As the one of Seehafer, (1978) our scheme is based on a Fourier expansion. However, we enforce periodicity by choosing an MHD-compatible symmetry condition for B_z at the x and y boundaries of the system with a periodic domain $-L_x \leq x \leq L_x$, $-L_y \leq y \leq L_y$ four times as large as the original region ($0 \leq x \leq L_x$, $0 \leq y \leq L_y$). The larger region is fully periodic by construction and the total magnetic flux through it is balanced to a high degree.

Due to the high-plasma-β state of the chromosphere and corona one is free to "fill" the initial magnetic field configuration with plasma, just in accordance with requirements for an equilibrium between the gravitational force density and kinetic plasma pressure. As for the temperature stratification one can use the most appropriate one, e.g. according to VAL (Vernazza et al., 1981). The resulting initial distribution of the plasma density in thermal equilibrium with the solar gravity assuming $g = const. = 275 m/s^2$ (since the pressure scale height is of the order of or even larger than the height of the simulated part of the corona), is shown in Figure 1 from Büchner et al., (2006). The Figure depicts

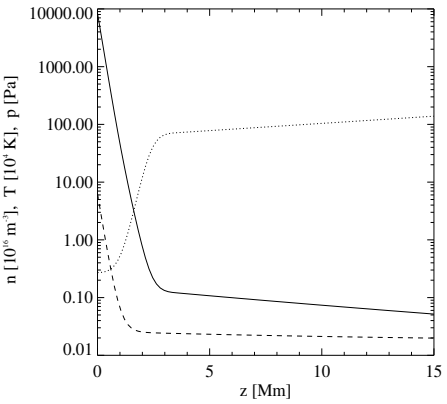

Figure 1. Initial height distribution of density (solid line), temperature (dotted line) and thermal pressure (dashed line). The gravitation is balanced by the thermal pressure. From Büchner et al. (2006).

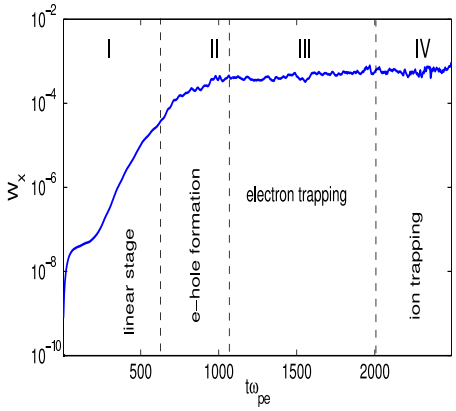

Figure 2. Vlasov-code simulated evolution of the electric field fluctuation energy at different stages of the linear (I) and nonlinear (II-IV) ion-acoustic current-driven instability. From Büchner & Elkina (2006b)

the initial distribution of the density (solid line) and of the thermal pressure (dashed line) which balances the solar gravity force density and the prescribed radially stratified temperature distribution (dotted line) here of the VAL model, but which also can be taken from observations.

3. Boundary Conditions

The energy which is released in the corona enters the solar atmosphere through the photosphere. In a simulation model the energy input from below the photosphere can be taken into account best by forcing the plasma in the chromosphere to move in accordance with the observed photospheric plasma motion. In a simulation model this idea can be implemented, e.g., by imposing a time-dependent motion of the chromospheric neutral gas derived from the observed plasma motion in and through the photosphere. Since in the chromosphere neutral gas and plasma are strongly coupled this way the observed photospheric plasma motion can elegantly be transferred, via plasma-neutral gas coupling, to the chromosphere. To implement this idea one has first to determine the photospheric plasma motion. A direct measurement is difficult since the typical flow velocities of the order of 1 km/s. Possibly emerging and submerging magnetic fluxes are too moving to slowly (Harvey et al., 1999) to be visible in Dopplergrams. Fortunately, in the photosphere plasma and magnetic flux are closely related due to the large magnetic Reynolds number (strong collisional resistivity). Hence, the photospheric plasma velocity field could be estimated, in principle, from the evolution of the magnetic fields. Several methods have been suggested to calculate the photospheric plasma motion from a sequence of photospheric magnetograms, e.g. by November & Simon, (1988), by Kusano et

al., (2002), by Welsch et al., (2004), by Longcope, (2004) and by Georgoulis & LaBonte, (2004).

The simplest is a local correlation tracking revealing a technique given the same name - LCT (November & Simon, 1988). The idea of the LCT method is to find the displacement that maximizes the spatially localized cross-correlation between two subsequently obtained magnetograms separated by a sampling time delay τ that is smaller than the lifetime of tracers in the scene. This method can be applied, if only the line-of-sight component of the photospheric magnetic field is available. Demoulin & Berger, (2003) have shown, however that local correlation tracking cannot distinguish a real horizontal displacement from apparent ones due to up- and downward plasma motion along inclined magnetic field lines. Based on geometrical arguments with B_h denoting the horizontal, the in-photosphere-component and and B_v the vertical component of the magnetic field, directed perpendicular to the photosphere, one can correct the LCT result using the relation

$$\vec{u}_h = \vec{v}_h - \frac{v_v}{B_v}\vec{B}_h, \tag{1}$$

where v_v and v_h denote the vertical and the horizontal components of the "real" velocity, while u_h is the horizontal component of the apparent velocity, in this case the LCT velocity, respectively.

If the full photospheric vector magnetic field information is available better results can be obtained by taking into account that the plasma motion should be consistent with the vertical component of the induction equation (Kusano et al., 2002; Welsch et al., 2004). An alternative technique is the minimum energy fit suggested by Dana Longcope, (2004). His method also uses the vertical component of the induction equation, but selects the solution by minimizing an energy functional. A comparison of the different methods applied to an active region on the sun is given in a companion paper published in this volume (Santos et al., 2006).

Using the this way obtained information about the photospheric plasma flow one can construct the boundary condition for the $Z = 0$ plane. For the X and Y boundaries one should implement MHD compatible line symmetric boundary conditions with respect to the center of each boundary plane as for the magnetic fields. For the upper boundary $Z =_{max}$ one should consider asymptotic boundary conditions with vanishing fields and flows.

In practice there are situations, where just a horizontal motion of the photospheric plasma is observed, i.e. without emerging or submerging fluxes. In this case one can impose a linear combination of neutral gas vortices chosen in accordance with the observed photospheric plasma motion as a boundary condition. If the velocity fields are chosen to satisfy $\nabla \cdot \mathbf{u}_n = 0$, the density will be conserved (incompressible neutral gas forcing). In this case the velocity field contained in the x, y plane is represented by a potential: $\mathbf{u}_n = \nabla \times (U\mathbf{e}_z)$. The contour lines of the function U are the streamlines of the flow, which should be taken from the observations. Although such neutral gas motion is specified throughout the whole simulation domain it is effective only where the collisional coupling between gas and plasma is sufficiently efficient, i.e. mainly in the chromosphere. The tangential velocity at the lower boundary is specified as defined by the neutral motion whose normal component is set to zero. In the example,

given in section section 6., this type of boundary condition is implemented after a rotation of a major magnetic flux concentration was observed below an EUV bright point by Brown et al., (2001).

4. Model Equations

In order to describe the coupling between photosphere and corona one has to take into account that the chromospheric plasma is denser and that the coronal plasma is hotter (see Figure 1). The chromosphere is, therefore, Spitzer-type collision dominated, and, in addition, in permanent interaction with the chromospheric neutral gas via charge exchange, ionization and recombination. Hence, in the chromosphere one has to consider the friction between plasma and neutral gas as well as the thermal contact between the two. The corresponding magnetohydrodynamic set of equations is given by:

$$\frac{\partial \rho}{\partial t} = -\nabla \cdot \rho \mathbf{u} - \mu(\rho - \rho_n) \tag{2}$$

$$\frac{\partial \rho \mathbf{u}}{\partial t} = -\nabla \cdot \rho \mathbf{u}\mathbf{u} - \nabla p + \mathbf{j} \times \mathbf{B} - \nu\rho(\mathbf{u} - \mathbf{u}_n) - g\rho \tag{3}$$

$$= -\nabla \cdot \left[\rho \mathbf{u}\mathbf{u} + \left(p + \frac{B^2}{2\mu_n}\right)\underline{\underline{1}} - \frac{\mathbf{B}\mathbf{B}}{\mu_n}\right] - \nu\rho(\mathbf{u} - \mathbf{u}_n) - g\rho \tag{4}$$

$$\frac{\partial \mathbf{B}}{\partial t} = \nabla \times (\mathbf{u} \times \mathbf{B} - \eta \mathbf{j}) \tag{5}$$

$$\frac{\partial p}{\partial t} = -\nabla \cdot p\mathbf{u} - (\gamma - 1)p\nabla \cdot \mathbf{u} + (\gamma - 1)S \tag{6}$$

$$\nabla \times \mathbf{B} = \mu_0 \mathbf{j} \tag{7}$$

The independent variables of equations (2) - (7) are the plasma mass density $\rho = n(M_i + m_e)$, where n is the number density of electrons and ions in a quasi-neutral plasma, the subscripts e and i stand for electrons and ions, respectively, where ions are mainly protons. Other independent macroscopic variables to be considered are the neutral gas mass density ρ_n, the plasma flow velocity $\mathbf{u} = \mathbf{u}_i + \mathbf{u}_e$ and the neutral gas flow velocity $\mathbf{u}_n$. To the lowest order it is appropriate to consider an isothermal plasma with equal electron and ion temperatures ($T_e = T_i = T$). Hence, the kinetic plasma pressure is given by $p = p_i + p_e = 2nk_BT$ and the electric current density as $\mathbf{j} = en(\mathbf{u}_i - \mathbf{u}_e)$. Another important simulation variable is the magnetic field $\mathbf{B}$ while the electric field can be expressed via the Ohm's law as $\mathbf{E} = -\mathbf{u} \times \mathbf{B} + \eta \mathbf{j}$ assuming that a macroscopic resistivity η exists. A combination of interactions via ionization, recombination and friction between plasma and neutral gas can be parameterized via general rates ν and μ. Assuming adiabaticity the polytropic index becomes $\gamma = 5/3$. For the gravitational acceleration one can use the surface value $g = 275 m/s^2$ as long as the pressure scale height is of the order of or even larger than the height of the simulated part of the corona. The energy equation (6), which closes the set of fluid equations, contains a source (and loss) function S. In dependence on the scope and purpose of the model one can contain some or all of the following terms:

$$S = \eta \mathbf{j}^2 - 2\kappa_T n k_B (T - T_n) - \nabla_\parallel \cdot \mathbf{q}_\parallel - L_r \tag{8}$$

The first term in expression (8) describes the Joule heating, characterized by the resistivity η, the second term is responsible for the thermal exchange between neutrals and plasma, parameterized by the heat conduction coefficient κ_T, the third term describes (parallel) heat conduction $q = \kappa_\parallel \nabla_\parallel T$ and the fourth term (L_r) quantifies the radiation losses. The factor two in front of the plasma-neutral heat exchange term arises from the assumption of equal electron and ion temperatures and from the assumption of equal exchange rates $\kappa_{Te} = \kappa_{Ti} = \kappa_T$. Since electron heat conduction exceeds the ion heat conduction by an order of magnitude one can neglect the latter to the lowest order, considering basically the electron heat conduction. As a result there is no factor two in front of the heat conduction term. The strongest heat conduction takes place parallel to the magnetic field. For the parallel electron thermal conductivity $\kappa_\parallel$ it is appropriate to consider the classical Spitzer-value $1.8 \cdot 10^{-10} T^{5/2} (\ln \Lambda)^{-1}\ Wm^{-1}K^{-1}$. With a Coulomb logarithm $\ln \Lambda \approx 20$ for typical solar temperatures one obtains $\kappa_\parallel \approx 10^{-11} T^{5/2}\ Wm^{-1}K^{-1}$. For typical coronal temperatures the radiation losses L_r can be parameterized as $n n_n Q_r(T)$ for which the temperature dependence $Q_r(T)$ was evaluated by a number of authors. The function Q_r, graphed, e.g. in (see, e.g. Priest, 1982, page 88, Fig. 2.2.), has a maximum around $T = 10^5$ K and a minimum near 10^7 K. An analytic approximation is $Q(T) = \chi T^\alpha\ Wm^3$, piecewise approximated by values of α and χ, which can be found in the literature (see, e.g. Priest, 1982, pp 88–89). In the chromosphere plasma and neutral gas are coupled by collisions, causing friction and energy exchange, but also by ionization of the neutrals and recombination of ions. The main role of these interactions is to maintain a strong coupling between plasma and the neutral gas in the chromosphere. In the transition region to the corona this interaction should vanish. To meet this requirement the exact values of the rates μ for the mass exchange and ν for the momentum exchange do not matter as long as they are sufficiently large compared to the characteristic time of changes, i.e. as long as $\nu \cdot \tau_{Ao} \gg 1$, where $\tau_{Ao} = L_0 / v_{Ao}$ is a characteristic Alfvén transit time for a typical length scale L_0. The ion neutral collision frequency is $\nu_{in} = n_n \sigma_n v_{th}$, where the cross-section σ_n depends on the type of the collisions and of the colliding particles. For elastic momentum exchange one can take assume a cross section for the neutral gas atoms $\sigma_n \approx 10^{-19}$ m^2. Assuming a coronal number density $n \approx \cdot 10^{15}$ m^{-3}, a magnetic field strength $B_0 = 1\text{G} = 10^{-4}\text{T}$ and a normalization scale length of $L_0 = 500$ km one finds $\nu \cdot \tau_{Ao} \ll 1$, i.e. there is practically no momentum transfer with the neutrals in the corona. In the much denser chromosphere $\nu \cdot \tau_{Ao} \gg 1$ leads to as strong coupling between the neutral gas and the plasma. Realistic values for the electron-ion collision rates ν_{ei} are about 10^7 s^{-1} in the chromosphere and $\nu_{ei} \approx 10^3$ s^{-1} in the lower corona.

5. Anomalous Resistivity

The correct macroscopic appearance of the microscopic field-particle momentum exchange, limiting the growth of currents and magnetic fields (cf. equation (5)

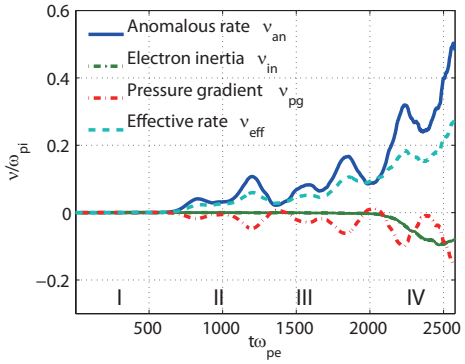

Figure 3. Effective collision rates, parameterizing the contribution of the irreversible interaction between electric field and particles as well as the contributions of electron inertia and pressure gradients to the electron momentum balance (Ohm's law). From Büchner & Elkina, (2006b).

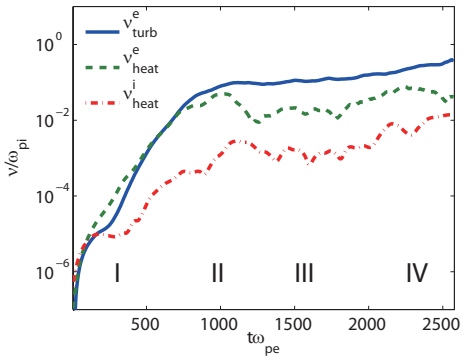

Figure 4. Effective collision rates, parameterizing the energy transfer to the electric fluctuations (solid line), the ion- (dash-dotted line) and electron heating (dashed line) in the course of the linear and nonlinear stages of the instability evolution. From Büchner & Elkina, (2006b).

) as well as the current induced heating (cf. equation 8) are concerned leads beyond the scope of a fluid theory. Traditionally the gap between the detailed, kinetic effect of current dissipation and its macroscopic consequences is closed by *ad hoc* models. One possible assumption (see, e.g., Neukirch et al., 1997) is a current density dependent resistivity with a switch-on current density threshold j_{crit}. As one can see in expression (9) in such model only currents, exceeding j_{crit} cause resistivity. For larger current densities the resistivity is considered to increase quadratically with the excess current density. Unfortunately, neither a current-density dependent threshold nor growing with increasing current densities resistivity is justified by any microscopic theory of resistivity. Also, as we will demonstrate in section 6.) such model indicates wrong locations of finite resistivity and, therefore, finite-B-reconnection in the real, three-dimensional world.

$$\eta = \begin{cases} 0 & \text{if } |\mathbf{j}| < j_{crit}, \\ \eta_0 \left(\frac{|\mathbf{j}|}{j_{crit}} - 1 \right)^2 & \text{if } |\mathbf{j}| \geq j_{crit}. \end{cases} \tag{9}$$

$$\eta = \begin{cases} 0 & \text{if } |u_{ccv}| < u_{crit}, \\ \eta_0 \left(\frac{|u_{ccv}|}{u_{crit}} - 1 \right) & \text{if } |u_{ccv}| \geq u_{crit}. \end{cases} \tag{10}$$

Instead of a current density threshold, microscopic theories of anomalously enhanced collisionless resistivity usually indicate that the average particle drift velocity, responsible for the current flow, does control the switch on of an enhanced net momentum exchange between the current carriers and the self-generated plasma turbulence. In this sense Yokoyama & Shibata, (1994) (see also Magara & Shibata, 1997) used a resistivity model as given by equation (10) to investigate the dependence of the resistivity on macroscopic, fluid parameters. Without any microscopic theoretical evidence they (see equation (10)) also assume that the resistivity further increases with a growing current carrier

velocity. Somov & Oreshina, (2000) adopted the empirical result of laboratory experiments of de Kluiver, et al. (1991) to assume a dependence of the anomalous resistivity on the electric field following $\eta = 10\eta_0 E/E_{Dr}$, where E_{Dr} is the Dreicer runaway electric field.

But what dependence of η on the macroscopic plasma parameters is justified best by the a microscopic theory? Since the coronal plasma-β is small (for usual coronal parameters like $B = 10^{-3}\,T$ and $n = 10^{15} m^{-3}$ one finds $\beta \approx 0.03$), i.e. electrostatic instabilities are possible candidates. As far as the coronal plasma parameters are concerned SUMER observations onboard the SoHO mission have shown that the electron temperatures in the corona are usually slightly less than $10^6\,K$ while the ion temperatures exceed $10^6\,K$, reaching up to $10^7\,K$. This excludes the generation of the ion-acoustic instability which requires $T_e \gg T_i$. Hence, the current carrier velocities must exceed the electron thermal velocity to excite the fluid-type electrostatic Buneman instability. From the microscopic electron momentum balance equation follows, after averaging the individual momentum exchange processes over appropriate temporary and spatial scales, a macroscopic resistivity, which can be used in an Ohm's law. The resulting irreversible momentum transfer away from the electrons can be parameterized by an effective "collision rate" ν_{eff}, which reveals a parameterization of the effective resistivity (Büchner & Elkina, 2006a):

$$\eta_{eff} = \frac{\nu_{eff}}{\epsilon_0 \omega_{pe}^2} \tag{11}$$

where $\omega_{pe} = \sqrt{ne^2/\epsilon_0 m_e}$ is the plasma frequency with $\epsilon_0 = 1/\mu_o c^2$ being the vacuum electric permeability. For the effective "collision rate" due to a current instability O. Buneman heuristically estimated $\nu_{eff} \approx \omega_{pe}/2\pi$ (Buneman, 1958). However, there no theoretical investigation could justify such a large effective collision frequency. Also, it was found that a reactive Buneman-type instability quenches itself within $\tau \cong 10/\omega_{pe}$, i.e. within a few electron plasma periods (Treumann, 2001). Hence the fluid-like reactive Buneman instability could at most pre-heat of electrons enabling a follow-up ion-acoustic instability. However, as we currently have shown by means of Vlasov-code simulations, this does not happen in the solar corona. Instead, the Buneman instability continues nonlinearly, enhancing the level of turbulence after an electron trapping stage via ion scale structure formation up to the formation of double layer structures (Büchner & Elkina, 2006b). Figure 2 taken from that paper depicts the evolution of the energy of the electric field fluctuations in the course of an ion-acoustic current-driven instability from the linear stage (I) to electron- and ion trapping as well as to double layer formation (stage IV, see, e.g., Büchner & Elkina, (2006b)). The resulting effective collision rates are depicted in Figure 3 for the different contributions to the electron momentum exchange, i.e. due to interaction with the self-generated fields (ν_{eff}, dashed line), due to the electron inertia and pressure gradient effects which all contribute to the electron momentum balance (Ohm's law, see, e.g., Büchner & Elkina, (2006b)). As far as the energy flow is concerned Figure 4 shows the effective exchange rates, parameterizing the energy transfer to the electric fluctuations (solid line), the ion- (dash-dotted line) and electron heating (dashed line) in the course of the linear and nonlinear stages of the instability evolution (Büchner & Elkina, 2006b). As one can see the efficient en-

ergy exchange rate coincides well with the momentum exchange rate so that the resulting resistivity obtained via ν_{eff} using equation (11) can be used in both, momentum and energy equations (5) and (8), respectively. With $\nu_{eff} \approx 0.5\omega_{pi}$ (where $\omega_{pi} = \sqrt{ne^2/\epsilon_0 M_i}$ is the ion plasma frequency, Büchner & Elkina, from 2006b) one obtains $\eta_{eff} \approx 1\,\Omega$m. This is 10^7 larger than the collisional resistivity of the same coronal plasma (see section 1.)! Hence, $R_m \approx 1$ can be reached, therefore, already for dissipation regions scaling as $L \approx \eta_{eff}/\mu_0 v \approx 250$m.

On the other hand, the critical threshold value $u_{crit} \approx v_{te}$ for the current carrier drift velocity, necessary to excite an ion-acoustic instability in nearly isothermal plasmas requires magnetic field gradient scales $l \approx B/\mu_0 nev_{te}$ of the order of $10\,m$ for solar parameters ($B = 10^{-2}\,T$, $n = 10^{15}m^{-3}$, $T = 10^6\,K$). The required magnetic field gradient scale becomes larger only in stronger magnetic fields, reaching $100\,m$ only in a $B = 10^{-1}\,T$, i.e. in a kG field. Another possibility is the excitation of lower-hybrid-drift or even drift-cyclotron instabilities. The LHD instability requires a weaker gradient scale than the ion-acoustic instability, of the order of $13(M_i/m_e)^{1/4}\,m$ in a $B = 10^{-2}\,T$ solar magnetic field. In weaker magnetic fields the length scale increases indirectly proportional to the field strength. For the electromagnetic ion cyclotron drift instability the gradient length scale requirement is also weaker, $13(M_i/m_e)^{1/2}\,m$, i.e. $(M_i/m_e)^{1/4}$ larger scale lengths (weaker gradients) are sufficient. Unfortunately, there is now reliable result known yet for the nonlinear evolution of these instabilities for solar coronal plasma conditions, i.e. neither the saturation amplitudes nor the anomalous collision rates are determined. There is hope that multi-dimensional kinetic theories and simulations, still to be developed, will reveal suffiently large amounts of anomalous resistivity resulting from lower-threshold instabilities like, e.g., the lower hybrid drift instability, or even electromagnetic instabilities like the drift-cyclotron instability.

6. Example

In two dimensions the influence of the macroscopic resistivity model on reconnection has been investigated, e.g., by Yokoyama & Shibata, (1994), Magara & Shibata, (1997) and Roussev et al., (2002). In contrast to, e.g. (Neukirch et al., 1997), these authors parameterized the resistivity in accordance with the current carrier velocity $u_{cc} = j/\rho_e$ (see equation (10)). The question is, whether these results apply also to the real 3D reconnection in the solar corona, its triggering, location and structure? Let us use the above described numerical simulation setup to derive the location where anomalous resistivity and, therefore, reconnection is triggered for different resistivity models for a solar corona which is modelled using observations of the photospheric magnetic field as initial and boundary conditions as described above. For definiteness we consider the well investigated case of a II phase of an EUV bright point observed by Brown et al., (2001). Deriving the initial and boundary conditions of the simulation from MDI magnetograms according to the LCT method we obtained the boundary conditions. We simulated the corona on a non-uniform grid with 107 points in the vertical direction (z) , and 131×131 grid points in the horizontal (periodic) x and y directions, all including two "ghost zones", additional grid planes, allowing the calculation of gradients on the boundaries. The simulation domain

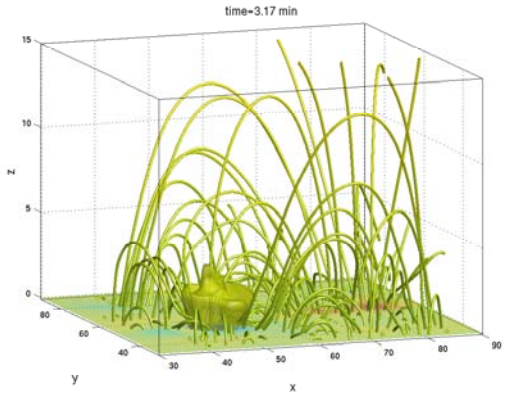

Figure 5. Isosurface of the resulting parallel current density $j_{par} = 7.5 j_{norm}$ embedded in the coronal magnetic fields. From Büchner et al. (2006).

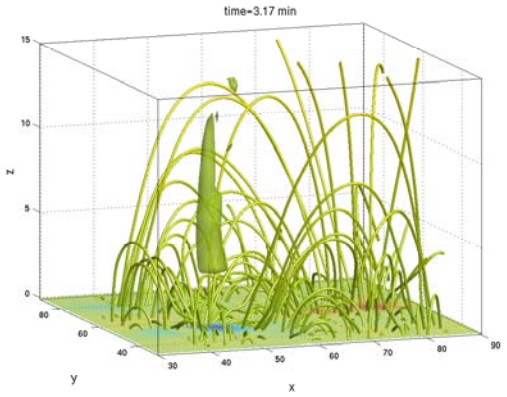

Figure 6. Isosurface $u_{ccv||} = 0.2 v_A$ of the parallel current carrier velocity embedded in the coronal magnetic fields. From Büchner et al. (2006).

covers a volume of $32 \times 32 \times 15$ Mm^3 (excluding the ghost zones), providing a non-equidistant vertical resolution between 150 km in the chromosphere and transition region and 800 km in the corona. The horizontal resolution was 500 km. Let us test the influence of the switch-on conditions of the anomalous resistivity for the two resistivity models - one based on a critical current density, like the one given by equation (9) and another, based on a critical value of the current carrier velocity as expressed by equation (10). In Figures 5 and 6 we depict the resulting isosurfaces of constant current densities (Figure 5) and of constant current-carrier velocity components parallel to the magnetic field $u_{ccv\|} = j/\rho = 0.2 v_A$, where v_A is the Alfvén-velocity. Note that both Figures are obtained from the same data set. The difference in the isosurfaces demonstrates that a resistivity model oriented at the current density would lead to current dissipation preferentially in the chromosphere (see Figure 5). Contrary, a microscopically justified current-carrier velocity based resistivity model would trigger reconnection first of all in the transition region and above within a narrow channel (see Figure 6).

7. Summary and Outlook

In order to maximize the output of Solar-B it is appropriate and timely to develop quantitative forward models of the coupling between photosphere, chromosphere and corona in order to verify 3D reconnection in the solar corona. Unfortunately, most of the existing models are not yet directly based on observations. We have described requirements and steps toward the development of genuine forward models based on time dependent photospheric magnetic field observations as they will be provided by SOT onboard Solar-B. Still work has to be done to complete the chain of steps necessary to simulate the EUV luminosity of the heated coronal plasma, which will be observed by EIS, and to obtain the X-ray intensity due to energetic particles, which will be observed via

by XRT. Here, in this paper, we especially addressed magnetic reconnection in the corona as a process releasing magnetic and plasma flow energy supplied from below the photosphere. Theoretically open is still the question of a realistic consideration of the coupling between not directly observable macroscopic variables and kinetic processes. Our fluid investigations have shown that the macroscopic resistivity model strongly influences the onset conditions, location and size of 3D reconnection regions. A macroscopic parameterization of the microscopic transport processes requires the determination of a threshold value for the current carrier velocity or the magnetic field gradient scale as well as an anomalous "collision rate" parameterizing the resistivity. Currently performed high-resolution Vlasov code investigations have shown that for solar conditions the threshold of known collisionless current instabilities necessary to create a sufficient amount of anomalous resistivity, still requires very strong gradients, i.e. filamented to small scales structures in order to excite sufficiently large electric fields (Büchner & Elkina, 2006a). However, future multidimensional considerations of obliquely propagating plasma turbulence modes and the resulting phase space structuring processes might help to resolve this dilemma.

Acknowledgments. The author gratefully thanks the organizers of the Solar-B mission for all their efforts, the organizers of the Kyoto meeting for their invitation, N. Elkina, B. Nikutowski and A. Otto for fruitful collaboration and especially the DFG for its support of the attendance of the author of the Solar-B meeting as well as of project BU 777/2. I wish the Solar-B mission much success!

References

Axford, W. I., 1984, *in: Reconnection in Space and Laboratory Plasma, AGU Geophys. Monogr., ed. E. Hones Jr.*, 4

Brown, D.S., Parnell, C.E., Deluca, E.E., Golub, L. & McMullen R.A., 2001, *Sol. Phys.*, 201, 305

Büchner, J., Nikutowski, B. & Otto, A., 2004a, *in "Multi-Wavelength Investigations of Solar Activity", Proc. IAU Symposium 223, eds. A. V. Stepanov, E. E. Benevolenskaya, A. G. Kosovichev, Cambridge University Press*, 223, pp 353–356

Büchner, J., Nikutowski, B. & Otto, A., 2004b, *in "Coronal Heating", Proc. SOHO-15, St. Andrews, 6-9 September 2004, ESA SP-575, eds. J. Ireland and R.W. Walsh*, pp 35–50

Büchner, J., Nikutowski, B. & Otto, A., 2005, *in "Particle Acceleration in Astrophysical Plasmas: Geospace and Beyond", AGU monograph 156, eds. D. Gallagher, J. Horwitz, J. Perez R. Preece and J. Quenby, AGU, Washington DC.*, pp 161–170

Büchner, J., 2006, *Space Sci. Rev.*, 122(14), 149160, doi:10.1007/s11214-006-8213-z

Büchner, J. & Elkina, N., 2006a, *Space Sci. Rev.*, 121(1-4), 237252, doi:10.1007/s11214-006-6542-6

Büchner, J. & Elkina, N., 2006b, *Phys. Plasmas*, 13, 082304, doi:10.1063/1.2209611

Büchner, J., Nikutowski, B. & Otto, A., 2006, *Astron. Astrophys.*, subm.

Buneman, O., 1958, *Phys. Rev. Lett.*, 1, 119

Cowling, T. G., 1957, *Magnetohydrodynamics, Interscience, New York.*

de Kluiver H., Perepelkin N. F., Hirose A., 1991, *Phys. Rep.* 199, No. 6, 281

Démoulin, P., Berger, A., 2003, *Sol. Phys.*, 215, 203

Georgoulis, M.K., LaBonte, B.J., 2004, *Astrophys. J.*, 615, 1029

Harvey, K. L., H.P. Jones, C.J. Schrijver & M.J. Penn, 1999, *Sol. Phys.*, 190, 35

Kusano, K., Maeshiro, T., Yokoyama, T., Sakurai, T. 2002, *Astrophys. J.*, 577, 501

Longcope, D.W. 2004, *Astrophys. J.*, 612, 1181
Magara T. & Shibata K., 1997, *Adv. Space Res.*, 19, No. 12, 1903
Neukirch T., Dreher J. & Birk G. T., 1997, *Adv. Space Res.*, 19, No. 12, 1861
November, L.J. & Simon, G.W., 1988, *Astrophys. J.*, 333, 427
Otto, A., Büchner, J. & Nikutowski, B., 2006, *Astron. Astrophys.*, subm.
Priest, E. R., 1982 *"Solar magneto-hydrodynamics", D. Reidel Publishing Company*, Dordrecht, Holland, 590 pp
Priest, E. R. & Forbes, T. G., 2000, *Magnetic Reconnection: MHD Theory and Applications* (Cambridge University Press)
Roussev, I., Galsgaard, K., Judge P.G., 2002, *Astron. Astrophys.*, 382, 639–649 doi: 10.1051/0004-6361:20011645
Sakurai, T., 1989, *Space Sci. Rev.*, 51, 11-48
Santos, J., Büchner, J., Alves, M. & Nikutowski, B., 2006, *this volume.*
Seehafer, N., 1978, *Sol. Phys.*, 58, 215–223
Shibata, K., 1998, *Astroph. Space Sci.*, 264, 1/4, 129–144
Somov, B.V. & Oreshina, A.V., 2000, *Astron. Astrophys.*, 354, 703–713
Solanki, S. K., Lagg, A., Woch, J., Krupp, N. & Collados, M., 2003, *Nature*, 425, 692–695
Spitzer, L., 1956, *"Physics of Fully Ionized Gases", Interscience, New York*
Treumann, R.A., 2001, *Earth Planets Space*, 53, 453–462
Tsuneta, S., 1996, *Astroph. J.*, 456, 840
Vernazza, J.E., E.H. Avrett & R. Loeser, 1981, *Astrophys. J. Suppl.*, 45, 635–725
Welsch, B.T., Fisher, G.H., Abbet, W.P. & Regnier, S., 2004, *Astrophys. J.*, 610, 1148OA
Yokoyama, T. & Shibata, K., 1994, *Astrophys. J.*, 436, L197-L200